Friction-induced energy losses in mechanical contacts subject to random vibrations

Vladislav Aleshin, Antonio Papangelo

Friction-induced energy losses in mechanical contacts subject to random vibrations

Vladislav V. Aleshin [a,b,*], Antonio Papangelo [c]

[a] Univ. Lille, CNRS, Centrale Lille, ISEN, Univ. Valenciennes, UMR 8520 – IEMN, LIA LICS/LEMAC, F-59000 Lille, France
[b] Tomsk State University, Tomsk, Russia
[c] Hamburg University of Technology, Department of Mechanical Engineering, Am Schwarzenberg-Campus 1, 21073 Hamburg, Germany

A B S T R A C T

In this paper, we apply the previously developed Method of Memory Diagrams (MMD) to the description of an axisymmetric mechanical contact with friction subject to random vibrations. The MMD belongs to a family of semi-analytical methods of contact mechanics originating from the classical Cattaneo–Mindlin solution; it allows one to efficiently compute mechanical and energetic responses to complex excitation signals such as random or acoustic ones. For an axisymmetric contact driven by random normal and tangential displacements having fractal statistical properties, we calculate the friction-induced mechanical energy loss averaged over a large number of realizations. In the considered problem, this energy depends on a very restrained number of parameters: on the rms of random displacements, on the fractal dimension, and on the upper cut-off frequency of the fractal spectrum. In addition, a radial distribution of the dissipated energy has been obtained that has a direct relation to wear in the contact system. For small displacement amplitudes, wear should be expected in an annulus inside of a mean contact circle whereas for large displacements it will start at the contact center.

1. Introduction

One of common manifestations of dry friction in mechanical systems is heat generation in vicinity of contact surfaces. Friction-induced heating results in a number of phenomena such as chemical transformations or melting; it also underlies various technologies including, for instance, friction stir welding and ultrasonic thermography for visualizing damage in solids. Another important process accompanied by frictional heating is wear i.e. formation of debris particles in the contact zone. In the classical Archard's model (Archard, 1953) of wear, the total volume of debris particles is proportional to the work of the friction force that produces the equal mechanical energy dissipation.

Certainly, these effects entirely depend on contact geometry and excitation. However, here we attempt to find a more general point of view at the problem and reduce as much as possible the number of parameters describing the system. This is possible by considering axisymmetric contact geometry and random vibrations. Then, by computing the work of the shear stress in the contact zone with the proper account for slip distances at every point, the desired friction-induced loss of mechanical energy can be obtained.

Based on the Amontons–Coulomb friction law, the classical Cattaneo–Mindlin solution (Cattaneo, 1938) for two spheres analytically links constant normal (N) and tangential (T) contact forces with constant normal (a) and tangential (b) displacements. Similarly, the Hertz-Mindlin solution (Mindlin and Deresiewicz, 1953) is common name for a series of analytical expressions applicable for the same contact geometry in the case when the forces evolve in accordance to several prescribed scenarios. More recently, four semi-analytical methods (Dobry et al., 1991; Jäger, 2005; Popov, 2017; Aleshin et al., 2015) have been developed that allow one to use arbitrary loading protocols in arbitrary convex axisymmetric (not necessarily spherical) geometries.

In this paper, we use the Method of Memory Diagrams (MMD) (Aleshin et al., 2015, 2018, 2019) in order to calculate the mechanical and energetic responses of an axisymmetric contact system. The friction-induced energy loss is averaged for a high number of realizations excited by random time-dependent normal and tangential displacements with certain statistical properties. Together with the analysis of the total energy loss, we also obtain its radial distribution in the contact plane. The latter quantity helps estimate where exactly in the contact zone wear will be most likely initiated.

* Corresponding author at: Joint European Laboratory LICS, IEMN, Univ. Lille.
E-mail address: vladislav.aleshin@univ-lille.fr (V.V. Aleshin).

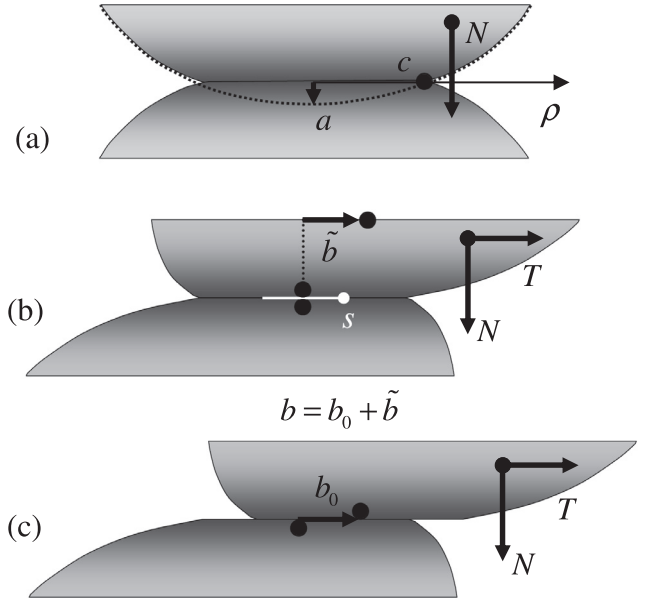

Fig. 1. Normal displacement a and two components of the total tangential displacement b: $\tilde{b}$_corresponds to a deformation of the bodies without sliding at the contact center, b_0 is a slip distance of the centers of contact areas of each body. Normal N and tangential T forces are applied to bulks of the bodies. (a) Only normal load applied. (b) Partial slip when the central area (white) of radius s is stuck. (c) Total sliding with no stick zone.

2. Cohntact forces and displacements

While a frictional contact is mechanically excited, three contact states can be encountered: contact loss (i.e. open contact), partial slip, and total sliding. Assuming $a>0$ for the bodies in contact (see Fig. 1(a)), this displacement becomes negative when contact is lost; in this case the contact forces $N=T=0$. In the state of total sliding, $a > 0$, $N > 0$, and $T=\pm\mu N$ according to the Coulomb friction law (μ is the friction coefficient) in which the sign depends on the slip direction and equals $\mathrm{sgn}\dot{b}$ where dot stands for time derivative. Finally, in the case of partial slip, some points in the contact area slide like in the previous state but some not, and $|T| < \mu N$ ($a > 0$, $N > 0$). For convex axisymmetric geometry, stick takes place in a circle of a radius s smaller when the contact radius c whereas slip occurs in the remaining part of the contact i.e. in the annulus (s, c).

An unavoidable question that arises when describing frictional contacts is which pair - forces or displacements - are to be used as drive parameters. Certainly, it is the force that measures the interaction of a system with its environment, but at the same time forces are hardly suitable as drive parameters for isolated frictional systems. Indeed, both for open contact and total sliding, a non-equilibrated tangential force arises. Therefore, some information on the environment should be provided such as elastic reaction of other bodies or inertia of the strained material. However, accepting that the system is driven by displacements, a simple quasi-static formulation can be built up that do not involve any accelerated movement nor information about system's environment.

First of all, the normal reaction $N=N(a)$ is postulated independently of any tangential interactions (Fig. 1(a)). The normal load N is defined for any a, in contrast to the force driven system in which the inverse function $a=a(N)$ is not defined for negative N (adhesionless contact with no pull-of force considered). Then, once the pair (a, b) is given, the solution for the open contact and total sliding states is immediately given by

$$(N, T) = (0, 0), \tag{1}$$

$$(N, T) = \left(N(a), \mathrm{sgn}\left(\dot{b}\right)\mu N(a)\right) \tag{2}$$

respectively.

In order to complete the description in the case of partial slip, more advanced reasoning should be applied. Partial slip for spheres loaded by some particular excitation scenarios is described by the Hertz-Mindlin solution (Mindlin and Deresiewicz, 1953). In a more general case when the normal interaction is given by generic $N(a)$ which is not necessarily Hertzian, and the excitation protocol is arbitrary, the MMD can be used.

3. Method of memory diagrams in 2D

The MMD allows one to calculate the tangential response of an axisymmetric contact system in the partial slip state provided its normal response $N=N(a)$ is known. The method starts with the known solution (Jäger, 1995) for a system loaded by a certain normal displacement a followed by the application of a tangential one b. The tangential response is given by

$$\begin{cases} b = \theta\mu(a - q) \\ T = \mu(N(a) - N(a = q)) \end{cases} \tag{3}$$

with

$$\theta = \frac{2 - \nu}{2(1 - \nu)}, \tag{4}$$

where ν is Poisson's ratio. Here q is a parameter corresponding to the radius s of the central stick zone

$$q = a(c)|_{c=s}, \tag{5}$$

where $a(c)$ is a function that links the normal displacement a and the radius c (see Fig. 1(a)) of the contact produced by this displacement. Here the positive direction of slip is assumed for definiteness. This solution (Jäger, 1995; Ciavarella, 1998) is frequently called the reduced elastic friction principle, since it expresses the tangential response as a difference of the normal and reduced normal responses, i.e. when a is substituted by the smaller value q in the latter component.

It is easy to verify that Eq. (3) can be rewritten in the form

$$\begin{cases} b = \theta\mu \int_0^a D(\alpha)d\alpha \\ T = \mu \int_0^a D(\alpha)\left.\frac{dN}{da}\right|_{a=\alpha} d\alpha \end{cases}, \tag{6}$$

where $D(\alpha)=1$ if $q < \alpha < a$ and 0 otherwise (see Fig. 2(a)). In the MMD, it is demonstrated that the integral solution Eq. (6) holds not only for constant displacements, but for an arbitrary displacement history as well (Aleshin et al., 2015). However, the integrand $D(\alpha)$, called memory function or memory diagram, is more complex in the general case (see Fig. 2(b)). The shape of the memory diagram follows changes in the loading history that represents a sequence of applied increments Δa and Δb.

The detailed algorithm elaborated by Aleshin et al., 2015, is based on Eq. (6) and uses the fact that slip propagates inward starting from contact periphery. The Amontons–Coulomb friction law in which the tangential load cannot exceed the threshold μN results in the inequality $|D(\alpha)| \leq 1$ for the memory diagram. It is also shown that the memory diagram contains horizontal and curvilinear sections. The former ones are created during the slip process when q moves towards $\alpha=0$, while the latter ones are generated in a so-called overloading (Aleshin et al., 2015) or complete overlapping (Jäger, 2003) regime occurring when $\Delta a > |\Delta b|/(\theta\mu)$ > 0 i.e. the contact area growth rate is higher than the inward slip propagation rate. Since slip propagates starting from the contact border and the contact zone growth dominates, slip does not develop at all.

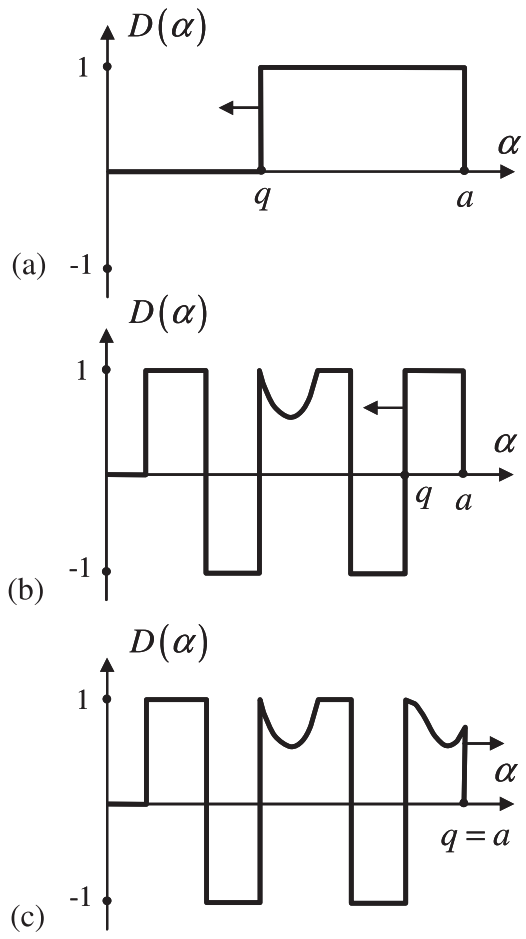

Fig. 2. (a) Memory diagram for constant loading corresponding to Eq. (3). (b) Typical memory diagram for an arbitrary loading history with a slip zone $q < \alpha < a$ in α-coordinates Eq. (7) that corresponds to $s < \rho < c$ in real geometric coordinates. (c) Particular case of overloading when slip is absent ($q = a$) and no mechanical energy is lost.

Horizontal and curvilinear sections can accumulate or erase each other following changes in the drive parameters (displacements). The power of the approach consists in the automated updating of a single internal memory function according to the prescribed rules instead of keeping track on complex shear stress and local displacement distributions in the contact zone.

The MMD is valid in the case of partial slip i.e. for $q > 0$. From Eq. (3) it immediately follows that $q = 0$ corresponds to $b = b_{\max} = \theta\mu a$ which is the maximum proper displacement that can be reached in the partial slip state. This maximum value represents the Coulomb friction threshold for the displacement-driven system, the analogue to $T_{\max} = \mu N$ for a system driven by force.

Here the MMD is formulated in α-coordinates related to the normal displacement,

$$\alpha = a(c)|_{c=\rho}, \tag{7}$$

where ρ is the radial coordinate in the contact zone (see Fig. 1(a)). Equations (6) can also be rewritten (Aleshin et al., 2015) using the real geometric ρ-coordinate.

The MMD requires the knowledge of the loading history in terms of a and b, as well as of the normal reaction $N(a)$ that actually accumulates all information on contact geometry, and has no free parameters. Having that in mind, it makes sense to denote the solution as

$$T = MMD(a, b). \tag{8}$$

The above result Eq. (8) implicitly uses an assumption that the system always stayed in the partial slip state i.e. the summits of the both bodies always stick. However, in reality the summits can separate because of total sliding or contact loss. In that case, to correct Eq. (8) it is necessary to introduce a tangential shift between the summits b_0 and the remaining displacement part $\tilde{b}$ arising due to proper tangential deformation of the bodies in contact. The repartition

$$b = b_0 + \tilde{b} \tag{9}$$

illustrated in Fig. 1 makes it easy to generalize the MMD solution in the partial slip regime altered by the other two contact states as

$$T = MMD\left(a, \tilde{b}\right). \tag{10}$$

Eq. (9) should be maintained in the contact loss and total sliding states as well, since entering the partial slip state requires the knowledge of $\tilde{b}$. In other words, at the moment of the partial slip beginning, the value b_0 should be memorized and kept constant until partial slip ends. The way of doing so depends on which state - contact loss or total sliding - preceded the current partial slip regime. In the former case $b_0 = b$ as the bodies were unstrained. In the latter situation, $b_0 = b - \mathrm{sgn}(\dot{b})b_{\max} \equiv b - \mathrm{sgn}(\dot{b})\theta\mu a$ since the proper tangential deformation of bodies was at maximum. With this remark, the description of the contact excited by an arbitrary displacement history becomes complete.

In addition to the load-displacement solution, the friction-induced energy loss can be analytically calculated for once a memory diagram is given. It is demonstrated by K. Truyaert et al., 2019, that the instantaneous work of the friction force produced by application of increments Δa and Δb equals

$$\Delta W = 2\mu(|\Delta b| - \theta\mu\Delta a)\left[N(a) - N(q) + (q - a)\left.\frac{dN}{da}\right|_{a=q}\right]. \tag{11}$$

This expression contains only variables present in the memory diagram (such as the one depicted in Fig. 2(b)) and also depends on the normal reaction curve. It is also possible to introduce the radial distribution $\Delta\varpi(\rho)$ of the incremental energy loss via

$$\Delta W = \int_s^c \Delta\varpi(\rho)2\pi\rho d\rho \tag{12}$$

which produces the result

$$\Delta\varpi(\rho) = 2\mu(|\Delta b| - \theta\mu\Delta a)\sigma(\rho)\left(1 - \frac{2}{\pi}\arcsin\left(\frac{s}{\rho}\right)\right) \tag{13}$$

in the form that explicitly contains geometry-related variables $\sigma(\rho)$ (normal stress distribution), the radius of the stick zone s, and the radial coordinate ρ. These expressions are to be used for calculation of heat generation by friction caused by random vibrations.

In conclusion it can be noted that the total dissipated energy do not depend explicitly on the contact system's geometry - all geometric information is contained in the normal response $N(a)$ - whereas the spatial energy distribution of the depends on the contact profiles shapes through $\sigma(\rho)$.

4. Excitation by random displacements

In the previous Section, the contact model has been formulated in a manner that requires as few parameters as possible. Now, we proceed in a similar way with random vibrations and introduce them with minimum parameters.

A good opportunity is presented by the concept of physical fractals. Mathematical fractal time-dependent curves have neither characteristic frequency nor a time scale. In practice, fractals can be obtained (Persson et al., 2005) by generating random curves

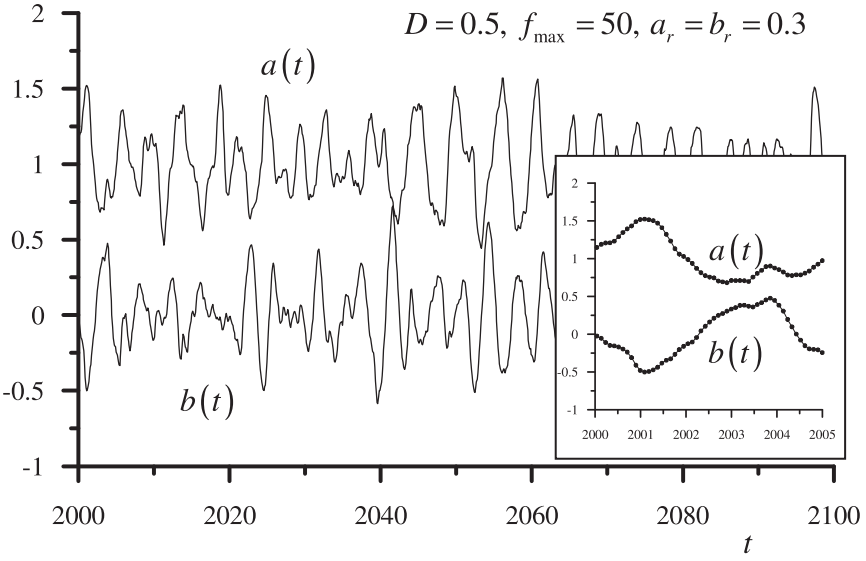

Fig. 3. Two fragments of the normal and tangential displacement histories generated via Eqs. (14)–(18).

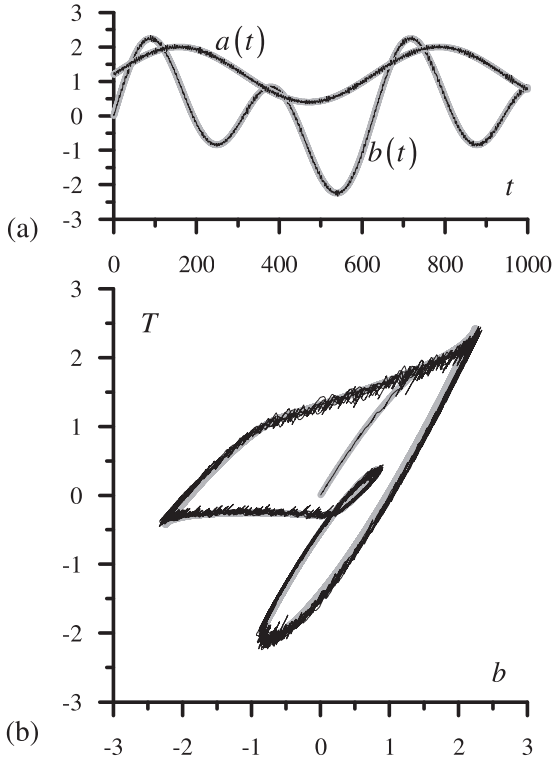

Fig. 4. Fragment of displacements history (a) and hysteretic tangential load-displacement response (b). The original deterministic periodic signals are plotted in thick gray lines, the noisy ones are represented by thin black curves.

with Gaussian distribution of heights and power law form of power spectral density. These two properties reflect the universality of fractals, since the power law spectrum has no characteristic frequency. However, since we actually deal with physical fractals, lower and upper cut-off frequency appear.

Fractal-type random vibrations on a precompressed contact have been numerically generated by setting

$$a(t) = 1 + a_r \zeta(t), \tag{14}$$

$$b(t) = b_r \xi(t), \tag{15}$$

where $\zeta(t)$ and $\xi(t)$ are independent random values having the Gaussian distribution with average 0 and standard deviation 1 at any t, and having a power spectral density

$$S(f) \sim \begin{cases} f^{-5+2D} & if \quad 1 < f < f_{\max} \\ 0 & otherwise \end{cases} \tag{16}$$

in accordance to Persson et al., 2005,[1] with D, fractal dimension. In such a representation, all quantities are normalized via the following substitutions:

$$\begin{aligned} &a \to \frac{a}{\bar{a}_0},\ b \to \frac{b}{\theta\mu\bar{a}_0}, \\ &N \to \frac{N}{\bar{N}_0},\ T \to \frac{T}{\mu\bar{N}_0}, \\ &t \to t\,\bar{f}_{\min},\ f \to f/\bar{f}_{\min}, \\ &W \to \frac{W}{\theta\mu^2\bar{N}_0\bar{a}_0}. \end{aligned} \tag{17}$$

These normalizations use two materials constants (θ fully determined by ν via by Eq. (4) and μ, friction coefficient) as well as three physical parameters of the system: the precompression displacement $\bar{a}_0$, the normal force $\bar{N}_0$ at this precompression, and the lower cut-off frequency $\bar{f}_{\min}$. As a result, the fractal random vibrations in the dimensionless form Eqs. (14)–(17) statistically depend only on the following three parameters: amplitudes a_r and b_r (supposed to be equal, $a_r = b_r$) normalized on the prestress displacement, fractal dimension D, and higher cut-off frequency normalized on the lower one.

The random profiles $\zeta(t)$ and $\xi(t)$ can be generated by calculating real and imaginary parts of the Fourier transform of the kind

$$\zeta(t) + i\xi(t) = C\int_{-\infty}^{+\infty} \sqrt{S(f)}\,(r_1(f) + ir_2(f))\exp(2\pi i f t)df, \tag{18}$$

where $S(f)$ is given by Eq. (16) for positive f, $S(f) = S(-f)$ for negative f, $r_{1,2}(f)$ are normally distributed and independent random numbers with zero mean, C is fixed to have unit standard deviation. In practice, C can be selected independently for each realization of $\zeta(t)$ and of $\xi(t)$ such that its rms equals 1.

[1] Appendix B of the cited paper by Persson et al., 2005, contains a power spectral density derivation for fractal surfaces, $C \sim f^{-2-2H}$, with the Hurst exponent $H = 3\text{-}D$. Following the same considerations on can get $C \sim f^{-1-2H}$ for fractal curves with $H = 2\text{-}D$ which finally results in Eq. (16).

The fractal dimension D is a number between 1 and 2 for a curve which is easy to verity using the classical box counting method Mandelbrot, 1983). This means that setting $1 < D < 2$ in Eqs. (14) and (15) produces fractal shapes for the curves of the displacements vs. time. However, it is also possible to consider fractal shapes for velocities or accelerations profiles corresponding to the actual contact displacements that excite the system. Since differentiation means spectrum multiplication by $2\pi if$, fractal shapes for velocity and acceleration curves are produced by the power spectral densities $S(f) \sim f^{-5+2D+2}$ and $S(f) \sim f^{-5+2D+4}$, respectively, which follows from Eqs. (16) and (18). Alternatively, one can still use $S(f)$ defined in Eq. (16) but set $0 < D < 1$ for fractal velocity profiles and $-1 < D < 0$ for fractal acceleration profiles. Hereafter we assume that D varies in the interval $(-1, 2)$ comprising the three cases referred to as the fractal acceleration, fractal velocity and fractal displacement, for the sake of brevity.

There are also two technical parameters of the random profiles: number of the points and the total observation time. The values used for all simulations presented in the paper are $2^{19} = 524288$ and $0 < t < 5000$, respectively. Fig. 3 shows two fragments of each displacement profile giving an idea about overall complexity of the signals and a number of points located at each monotonous section of the profiles (see inset).

5. Friction-induced energy losses

It is of interest to study frictional contact excited by random signals in two cases: where the signal is regular but contains a noise component and where it is completely random (no regular component). These situations are considered below in more detail. The examples are given for a contact of two spheres having the normal reaction $N = a^{3/2}$ in the normalized variables. At the end of this section, results for the radial distribution of the dissipated energy are presented in which the radial parameters ρ, c and s are normalized on $\bar{c}_0 = \sqrt{\bar{a}_0/R}$, the dimensional contact radius at normal displacement $\bar{a}_0$. This means that in order to retrieve the physical radial values from the dimensional ones, it is necessary to know the radius R of the spheres as well. However, the number of free parameters of the problem is not affected by this fact; the results described below depend only on $a_r = b_r$, D, and $f_{\max}$.

5.1. Deterministic vibrations with random noise

The former case is related to the question of the energy loss localization in contact systems. The matter is that the mechanical energy can be dissipated by friction only in the slip zone $s < \rho < c$ i.e. $q < \alpha < a$ in α-coordinates in which s or q shifts towards the contact center. Each time when Δb changes sign, the slip process develops again starting from the contact border $\rho = c$ ($\alpha = a$). This means that in order to reach inner parts of the contact area, a long monotonous intervals of $b(t)$ are needed. But the presence of noise can seriously reduce the chance of having monotonous internals. So will the presence of noise affect the energy loss localization? Actually, noise is unavoidably present in any real signal, therefore this issue has a universal character.

To exemplify the behavior of frictional contacts excited by noisy signals, we added noise with $a_r = b_r = 0.03$ amplitude to deterministic displacements profiles, namely to a monofrequency $a(t)$ and to $b(t)$ each composed of two sinewaves. Other parameters were kept as in Fig. 3:$D = 0.5$, $f_{\max} = 50$. Fig. 4(a) shows the noise component of the signal while Fig. 4(b) illustrates its influence on the tangential load-displacement response that remains moderate under the low noise amplitude applied. However, the total dissipated energy substantially increases (Fig. 5(a)) when noise is added. This is not surprising since the addition of noise also enlarges the total paths traveled by contact zone points of one body relatively to

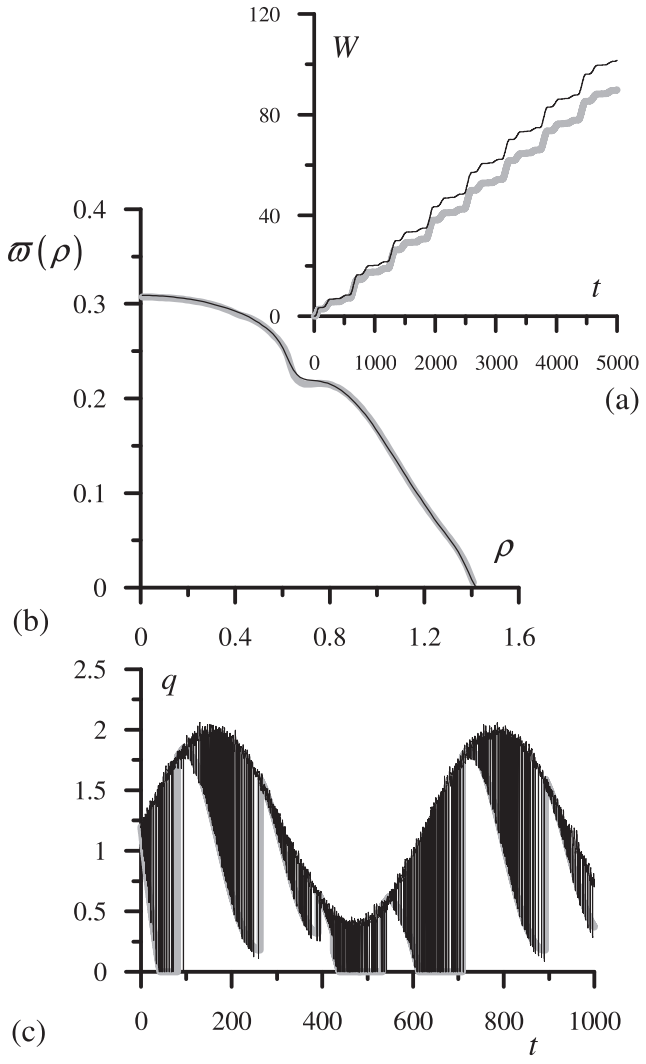

Fig. 5. Total dissipated energy (a) and its radial distribution (b) plotted for two spheres in contact. Plot (c) represents a fragment of the time dependence of parameters q characterizing the boundary between stick and slip zone. In all graphs, data for signals with and without noise are plotted in thin black and in thick gray line, respectively.

neighboring points of the other one. At the same time, the radial distribution of the dissipated energy stays approximately the same (Fig. 5(b)) while the behavior of $q(t)$ becomes completely different (Fig. 5(c)). Indeed, the boundary between the stick and slip zone quickly pulsates when noise is added, since, as it was already mentioned, instead of one long monotonous interval of the regular drive displacement the noise excitation signal has a multitude of small ones. This is clearly not a physical instability because it is not a physical quantity that rapidly changes but a configuration of zones where different boundary conditions apply. As a result, the considered problem of frictional contact between deformable solids remains well-posed.

5.2. Random vibrations

In this section, we consider a situation when the frictional contact is excited by purely random signals of the same kind as in Fig. 3, i.e. with no deterministic component. Since the statistical properties of random signals described in Section 3 do not depend on time, the average dissipated power P should be constant,

$$\langle W(t) \rangle = Pt, \quad P = const. \tag{19}$$

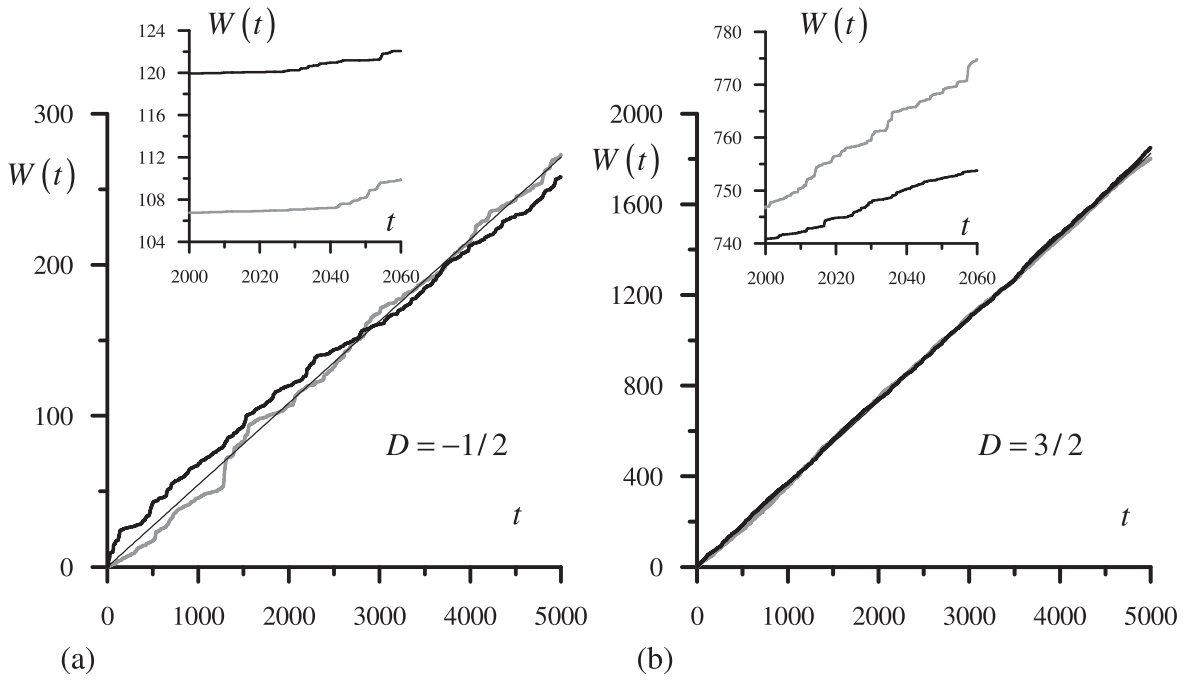

Fig. 6. Total dissipated energy W as a function of time t: two different realizations (gray and dark gray) and the average Pt for 50 realizations (thin black line) are plotted. Plots (a) and (b) correspond to $D = -1/2$ and $D = 3/2$, respectively. In the insets, fragments of $W(t)$ are zoomed in.

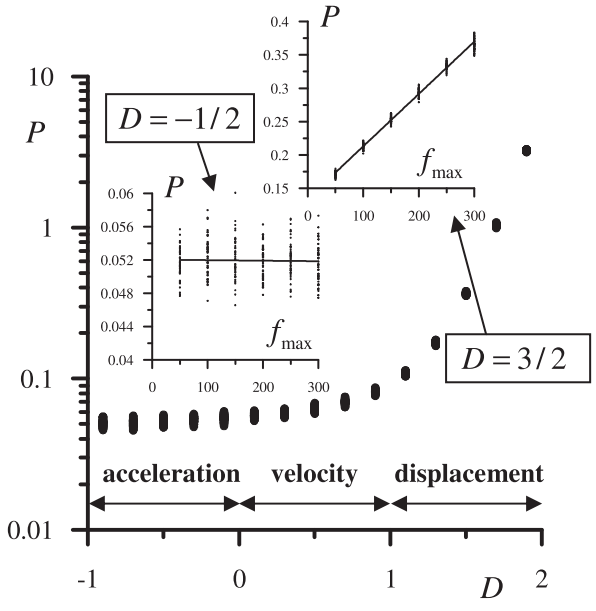

Fig. 7. Dissipated power as a function of parameter D. Three ranges marked at the bottom indicate which kind of signal has the fractal properties for corresponding values of D: acceleration, velocity, or displacement. The calculations are performed for $a_r = b_r = 0.3$, $f_{max} = 300$. The dependences of P on f_{max} are shown in insets for $D = 3/2$ and $D = -1/2$.

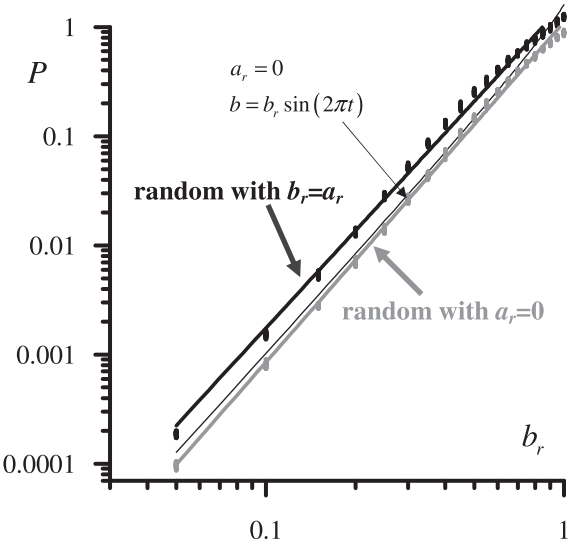

Fig. 8. Amplitude dependence of the average dissipated power P on the random vibration amplitude b_r. Three cases are considered: $a_r = b_r$, $a_r = 0$, and harmonic excitation with the tangential amplitude b_r while the normal one equals one ($a_r = 0$).

In Fig. 6, this fact is illustrated in more detail for two particular values of parameter D: $D = -0.5$, fractal acceleration, and $D = 1.5$, fractal displacement. It is easy to see that increasing D amplifies high frequencies in the power spectrum density Eq. (16) that produces an obvious effect on $W(t)$ realizations: for low D low-frequency random trends become pronounced while for higher D they disappear so that the realizations tend to the average. This behavior is additionally illustrated in the insets in Fig. 6. In addition, for larger D the increased contribution of higher frequencies results in the increase of the dissipated power P, just because the total relative distance traveled by bodies is larger. This feature is easy to see in Fig. 7 where the dependence $P(D)$ is plotted. Each "point" in their figure actually represents 50 agglomerated points corresponding to 50 realizations. The vertical length of all agglomerated points characterizes variability in data. This variability is much less for higher D which is shown in the both Figs. 6 and 7. In the insets of the latter figure, the effect of D on the dependence the upper cut-off frequency f_{max} is plotted. Non-negligible for fractal displacements, it is practically absent for fractal accelerations.

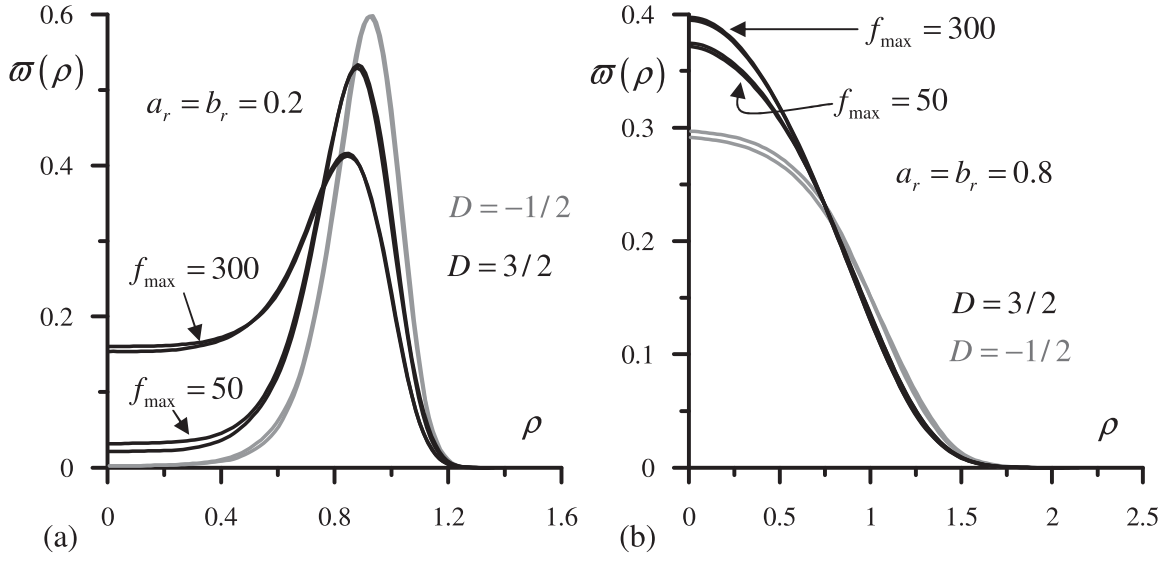

Fig. 9. Normalized dissipated energy density for weak ($a_r = b_r = 0.2$, plot (a)) and strong ($a_r = b_r = 0.8$, plot (b)) vibrations, for two values of parameter D corresponding to fractal acceleration ($D = -1/2$, in gray) and displacement ($D = 3/2$, in black). In the case of fractal displacements, examples two upper cut-off frequencies, $f_{\max} = 50$ and $f_{\max} = 300$ are given, while for fractal accelerations they practically coincide. Two realizations for each set of parameters are shown.

This means that the results for fractal accelerations are more universal in some sense, since they are affected by a smaller number of case-dependent parameters.

As it was shown P depends on D and additionally on f_{max} for higher D approximately in the range $1 < D < 2$ (for fractal displacements). The remaining point to examine is the amplitude dependence shown in Fig. 8 for fractal accelerations with $D = -1/2$ in the double logarithmic scale. When the normal amplitude is maintained constant (equals one in the normalized variables), the dissipative contact properties are almost the same as for the harmonic excitation at the lowest frequency $f = 1$ of the fractal spectrum. It can be shown using results obtained by K. Truyaert et al., 2019, that for the harmonic excitation of the kind

$$b(t) = b_H \sin(2\pi t)$$

the dissipated energy per period is equal in the dimensional variables to

$$W_H = \frac{32\mu^2\theta E^*}{15R^2}\left(c^5 - s_H^5 - 5c^3 s_H^2 + 5c^2 s_H^3\right) \tag{20}$$

with

$$b_H = \frac{\mu\theta}{R}\left(c^2 - s_H^2\right). \tag{21}$$

The corresponding power as a function of b_h taken equal to b_r was added to Fig. 8 for comparison. It can be seen that the application of the fractal acceleration signal and of the harmonic signal with $f = 1$ under constant compression dissipate approximately the same power, while assuming a random component of the normal displacement with the same amplitude slightly increases the dissipation efficiency. In all three cases, the dissipated power remains comparable, since for the fractal acceleration low frequencies close to $f = 1$ dominate in the spectrum. Certainly, this is not so for the fractal displacement excitation those dissipation is about 10- times higher (Fig. 7) in the considered example.

A linear approximation in the double logarithm scale shown that the curves in Fig. 8 roughly follow the power law with the power of about 3. More precisely, the power approximately equals 3.14 for the harmonic tangential excitation, 3.11 for the random tangential excitation, and 2.96 while exited by the normal and tangential signals simultaneously. Power 3 can be easily retrieved analytically in the harmonic case Eqs. (20), (21) by calculating

$$W_H \sim b_H^3 + o\left(b_H^3\right)$$

for small b_H.

As a final point, a radial distribution of the dissipated power is studied as a function of all parameters, i.e. of the excitation amplitudes $a_r = b_r$, of the fractal dimension D, and of the higher cut-off frequency $f_{\max}$. Here the most important is the dependence of the vibration amplitude. For all values of D and $f_{\max}$, at low amplitudes most of the energy dissipation occurs in an annulus located inside the average contact zone $\rho < \langle c \rangle = 1$, while at high amplitudes it primarily happens in a central circle. This fact is illustrated in Fig. 9 in which a normalized radial form-factor $\varpi(\rho)$ is plotted. In this figure $\varpi(\rho)$ is normalized in order to have

$$\int_0^c \varpi(\rho) 2\pi\rho d\rho = 1$$

for each realization. It can be also noted that the dependence of $\varpi(\rho)$ on a particular realization is quite weak, since $\varpi(\rho)$ is the total energy density accumulated during the whole observation time i.e. is a result of time averaging.

In fact, the energy dissipation localization in an annulus and in a circle for different random vibrations amplitudes is an expected result. Indeed, for small aptitudes the contact system stays in the state of partial slip when parameters s or q in Fig. 5(c) do not reach zero, therefore dissipation occurs only in the annulus where actual slip takes place. However, when slip progresses to the contact center at high excitation amplitudes, the energy dissipation in there becomes dominating since the contact is strongly compressed at the center.

6. Conclusions and summary

In this paper, we attempted to formulate and numerically solve the problem of friction-induced mechanical energy dissipation in contact systems subject to random vibrations. Amongst a multitude of contact geometries and possible statistical properties of vibrations, we have selected a case characterized by a very restrained

number of parameters, namely the prestressed contact of two equal spheres exited by random displacements whose time dependences have fractal properties. In this case, the mechanical and energetic response of the contact system depends only on the normal and tangential rms amplitudes (taken equal), on the higher cut-off frequency of the power spectral density, and on the fractal dimension understood in an extended way that comprises fractal shapes for the displacement, velocity, or acceleration curves. The calculations can also be performed for any other axisymmetric contact geometry, not necessarily spherical. The numerical method used is based on the semi-analytical solutions valid in all three contact states encountered: contact loss, total sliding, and partial slip. In the latter case, when some parts of the contact zone slip and some do not, the Method of Memory Diagrams has been applied.

The numerical study included two particular cases where the random component represents noise added to a regular deterministic excitation protocol, and where the excitation is purely random. In the former case, a stable behavior of the contact system has been observed when all physical parameters change slightly provided the noise amplitude is small. The only exception found is the radius s of the boundary between the stick and slip zones that dramatically oscillates even for weak noise. However, this parameter is not related directly to the physical reaction of the contact system and just determines the zones in which different boundary conditions apply.

In the latter case of the purely random vibrations, the average dissipated power is constant in time. Its value depends on the frequency content of the spectrum and becomes considerably higher when high frequencies are importantly present (fractal displacement excitation curve). In addition, the result strongly depends on the higher cut-off frequency in this case. In the opposite situation of weak high frequencies (fractal accelerations), this dependence practically disappears, and the dissipated power approximately corresponds to the case of a harmonic excitation at the lowest frequency of the spectrum. For increasing random amplitudes, the power increases approximately following the cubic law.

Another expected result concerned the radial distribution of the dissipated energy. For weak vibrations, the dissipation mostly occurs in an annulus located inside the average contact circle. The annulus shrinks and shifts towards the contact center with the increasing amplitude and finally becomes a circle.

Acknowledgements

The work was supported by the French National Center for Scientific Research (CNRS) and by the Tomsk State University competitiveness improvement program. We thank also the Center of Excellence in Computational Mechanics, director Prof. M. Napolitano, for sponsoring V.A.'s visit to Bari. A.P. is thankful to the DFG (German Research Foundation) for funding the project PA 3303/1-1. The authors are grateful to Prof. M. Ciavarella for simulating discussions.

References

Aleshin, V., Delrue, S., Trifonov, A., Bou Matar, O., Van Den Abeele, K., 2018. Two dimensional modeling of elastic wave propagation in solids containing cracks with rough surfaces and friction - Part I: theoretical background. Ultrasonics 82, 11–18.

Aleshin, V., Matar, O.B., Van Den Abeele, K., 2015. Method of memory diagrams for mechanical frictional contacts subject to arbitrary 2D loading. Int. J. Solids Struct. 60, 84–95.

Aleshin, V.V., Delrue, S., Van Den Abeele, K., Bou Matar, O., 2019. Nonlinear and hysteretic constitutive models for wave propagation in solid media with cracks and contacts. In: Kundu, T. (Ed.), Nonlinear Ultrasonic and Vibro-Acoustical Techniques For Nondestructive Evaluation (Chapter 5), p. 277.

Archard, J.F., 1953. Contact and rubbing of flat surface. J. Appl. Phys. 24 (8), 981–988.

Cattaneo, C., 1938. Sul contatto di due corpi elastici: distribuzione locale degli sforzi. Rend. Accad. Naz. Lincei. 27 (6), 342–348.

Ciavarella, M., 1998. The generalized Cattaneo partial slip plane contact problem. I-theory. Int. J. Solids Struct. 35 (18), 2349–2362.

Dobry, R., Ng, T., Petrakis, E., Seridi, A., 1991. General model for contact law between two rough spheres. J. Eng. Mech. 117 (6), 1365–1381.

Jäger, J., 1995. Axi-symmetric bodies of equal material in contact under torsion or shift. Arch. Appl. Mech. 65 (7), 478–487.

Jäger, J., 2003. Properties of equal bodies in contact with friction. Int. J. Solids Struct. 40, 5051–5061.

Jäger, J., 2005. New Solutions in Contact Mechanics. WIT Press, UK, p. 2181.

Mandelbrot, B., 1983. The Fractal Geometry of Nature. W.H. Freeman, p. 1145.

Mindlin, R., Deresiewicz, H., 1953. Elastic spheres in contact under varying oblique forces. J. Appl. Mech. (20) 327–344.

Persson, B.N.J., Albohr, O., Tartaglino, U., Volokitin, A.I., Tosatti, E., 2005. On the nature of surface roughness with application to contact mechanics, sealing, rubber friction and adhesion. J. Phys. 17, R1–R62.

Popov, V., 2017. Contact Mechanics and Friction: Physical Principles and Applications, 2nd edition, p. 277.

Truyaert, K., Aleshin, V.V., Van Den Abeele, K., Delrue, S., 2019. Theoretical calculation of the instantaneous friction-induced energy losses in arbitrarily excited axisymmetric mechanical contact systems. Int. J. Sol. Struct. 158, 268–276.